# Performance of Gas Fed Pulsed Plasma Thrusters Using Water Vapor Propellant*

John K. Ziemer†
Jet Propulsion Laboratory, M/S 125-109
California Institute of Technology
4800 Oak Grove Drive, Pasadena, CA 91109
(818) 393-4582, John.K.Ziemer@jpl.nasa.gov

Rodney A. Petr‡
Science Research Laboratory, Inc.
Sommerville, MA 02143

AIAA-2002-4273 §

## Abstract

The performance of two gas-fed pulsed plasma thrusters (GFPPTs) using both argon and water vapor for propellant has been measured using the JPL microthrust stand. The GFPPTs are designated as PT8 and PT9 with parallel plate electrodes, 65-130 $\mu$F of capacitance, 2-4 J per pulse, and between 0.1 - 4.0 $\mu$g of propellant per pulse. Performance measurements taken at JPL using argon propellant matched previous measurements taken at Princeton (EPPDyL) at the same conditions. As expected for an electromagnetic accelerator, efficiency scales linearly with exhaust velocity and the GFPPT Characteristic Velocity for both argon and water vapor propellants. Maximum performance was found using water vapor at the lowest mass bit value with PT9: efficiency near 20%, specific impulse near 7000 s, and impulse-to-energy near 6 $\mu$Ns/J. In general, performance using water vapor exhibits between 15-25% improvement over argon at the same operating conditions. Models of discharge conductivity and current sheet canting are reviewed to explain the measured differences.



†Staff Engineer, Advanced Propulsion Technology Group. Member AIAA.

‡Senior Engineer. Member AIAA.

§Presented at the 38th AIAA Joint Propulsion Conference, Indianapolis, IN, July 2002.

## 1 Introduction

Science Research Laboratory, Inc. (SRL) has been designing and testing gas-fed pulsed plasma thrusters (GFPPTs) since 1995. In coordination with the Electric Propulsion and Plasma Dynamics Laboratory (EPPDyL) at Princeton University and the Advanced Propulsion Technology Group (APTG) at JPL, nine generations of GFPPTs have been studied to date [1, 2, 3, 4]. The most recent designs have included modern solid-state pulsed power conditioning technology, new electrode geometries, and a new discharge circuit design to increase thruster performance [4]. These modern GFPPT designs are well suited to spacecraft where the $\Delta V$ requirement over the mission is large, demanding a high specific impulse to reduce the necessary propellant mass [5]. GFPPT technology also has the potential to enable some missions where a unique type of propellant is available for consumption.

The DARPA Orbital Express mission is one example where the propellant, in this case water, is chosen for its ease of storage and transport with the possibility that the satellites could be refueled on orbit. Although other propulsion technologies can also use water as a propellant, the GFPPT has the potential to provide the highest value of specific impulse which would allow for a wider range of maneuvering scenarios. To shorten maneuver duration, a large value of thrust-to-power ($> 10\mu N/W$) along with higher power operation ($> 1kW$) is required [5]. To investigate this possibility, we have used previously developed GFPPT performance models (See Ref. [6]) to de-

Figure 1: Picture of PT9 on JPL microthrust stand.

sign the next generation of GFPPT, PT10. Before completion, however, we have tested two previous GFPPT designs, PT8 and PT9, to verify performance measurement techniques and develop a water vapor propellant control system at JPL. This paper focuses on comparing the performance between argon and water vapor propellants with PT8 and PT9, including comparing measurements taken at EPPDyL and JPL using PT9 and argon. Measurements of the effective plasma resistance and a current sheet canting model developed by Markusic [7] are used to explain the differences between argon and water vapor performance.

We begin our paper with a brief discussion of the GFPPTs used in this study along with the microthrust performance measurement facility at JPL. We then present the performance measurements taken both at EPPDyL and JPL using argon and water vapor with PT8 and PT9. A model for electromagnetic acceleration in a GFPPT is used to investigate potential causes for the observed increase in performance using water vapor including changes in the effective plasma resistance and current sheet canting angle.

# 2 GFPPT Descriptions

The GFPPTs tested in this work (PT8 and PT9) have been described in the literature before (see Ref. [4], and only brief descriptions of the thrusters will be given here. The JPL Microthrust Stand has been described in detail in Ref. [8] and was used for all the performance measurements presented in this paper except where noted. PT9 is shown mounted on the JPL Microthrust Stand in Fig. 1.

## 2.1 PT8: Quad Thruster

PT8 is a slightly flared[1] parallel-plate GFPPT that belongs to the group of GFPPTs including PT6 and PT7 called the "quad thrusters" which are explained in more detail in ref. [3]. PT8 Combines four sets of electrodes mounted orthogonally on one 63 $\mu$F capacitor storage unit (energy bit near 2 J/pulse), with a total mass of 1.6 kg. Compared to the first quad designs, PT8 has a compact set of electrodes with a varying height-to-width ratio (close to 0.5), an RF discharge initiation system, and a ferrite yoke to reduce magnetic field fringing effects and contain the plasma in the electrode volume.

PT8 was used to test the effect of propellant type on performance using argon and water vapor. Water vapor was fed at a constant mass flow rate using the vapor pressure of water at room temperature and a sonic orifice. The mass bit value was varied by changing the time between pulses in a burst.

## 2.2 PT9: Variable $L'$

PT9 uses a modular set of parallel-plate electrodes for testing various values of inductance-per-unit-length. In all the tests reported here, the electrodes were 1/8" thick 70% tungsten 30% copper plates in the 1" x 1" (height x width) configuration with boron nitride plates insulating the outer surfaces not exposed to the discharge. This configuration has an inductance-per-unit-length, $L'$ = 3.9 nH/cm, and a capacitance of 130 $\mu F$ providing between 3.5-4.0 J/pulse.

For discharge initiation, PT9 uses a high voltage (2 kV) low energy (50 mJ) surface discharge spark over graphite and aluminum shavings bonded with epoxy. Although erosion rates have yet to be measured accurately for this thruster, visible damage to thruster components is greatly reduced compared to damage seen in life-tests with the surface-discharge plugs used in PT5 through PT8 [9].

As described in the next subsection, the water vapor mass flow rate itself can be controlled in the new JPL setup. This allows multiple mass bit values to be tested with a constant pulse rate for more similar operation between propellant types.

# 3 Performance Measurements

The performance measurement techniques have been described in Refs. [2, 4, 8] and will only be summarized

[1] Although PT8 has slightly flared electrodes with expansion angles of $< 10°$, they will be classified here using the conventional term "parallel-plate". This causes the inductance-per-unit-length, $L'$, to be variable along the thrust axis

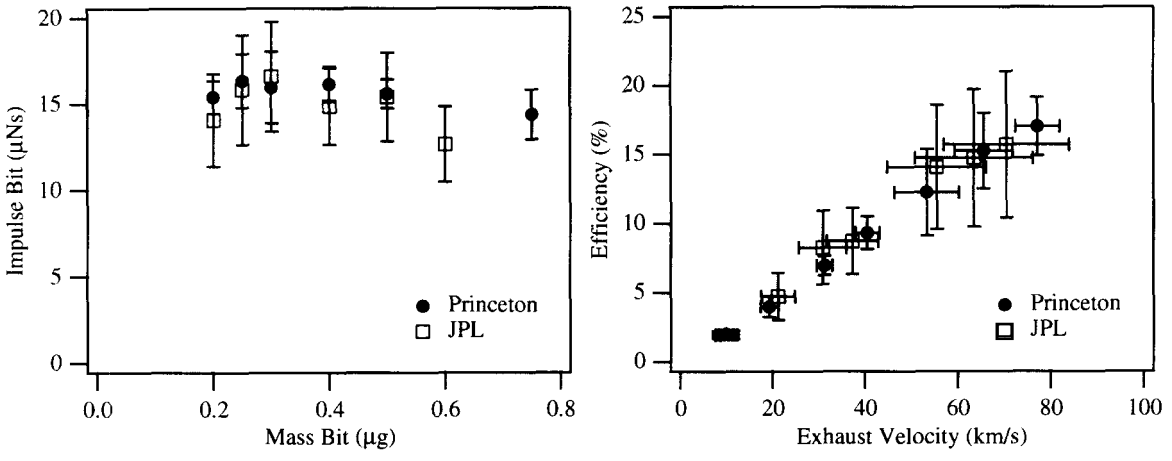


Figure 2: Performance taken using argon propellant at Princeton and JPL. The performance measurements agree within the error bars, and the trend of efficiency scaling with exhaust velocity is present in both measurements.

here. Most, if not all, techniques used at JPL are similar to those used at EPPDyL for measuring GFPPT performance. All measurements taken at JPL are conducted in a cryo-pumped stainless steel chamber with a base pressure of $10^{-6}$ Torr.

Mass flow rate is calculated by measuring the plenum pressure upstream of a sonic orifice and controlled by a solenoid valve just upstream of the thruster. For argon propellant, the plenum pressure is maintained by a regulator, while for water vapor the plenum pressure is regulated by a closed-loop heater control circuit. The timing of the propellant valve is set to just fill the electrode volume before the first pulse, with steady flow occurring until the burst is complete.

The impulse provided by each burst is found using the JPL Microthrust Stand by measuring the change in velocity before and after the burst. The impulse of the cold gas (spark plugs are not fired) is measured at each mass bit (pressure) setting and subtracted from the hot impulse measured when the capacitor is actually discharged. At least 1000 hot pulses are fired before any data is taken to clean electrodes of potential contaminants. Each mass bit value or condition is tested over at least 20 trials to provide statistical information. The average impulse bit is found by taking the total impulse from a burst and dividing by the number of pulses in a burst.

The energy on the capacitor is found by measuring the voltage before and after each pulse. Any voltage left on the capacitor bank after a pulse is recovered and used for the next pulse in the burst. The energy of each pulse in the burst is measured independently, and, similarly to the impulse bit measurement, an average value is used to determine performance.

Definitions of exhaust velocity, efficiency, and impulse-to-energy ratio follow normal conventions for pulsed thrusters (see Section 4 for more exact performance relations). The rest of this section includes a comparison of measurements taken at EPPDyL and Princeton using the same thruster and conditions with argon propellant. We also present the results from PT8 and PT9 using both argon and water vapor propellants in this section.

## 3.1 Comparison Between Princeton and JPL Measurements of PT9

Performance of PT9 in the 1" x 1" (b) configuration using argon propellant has been measured previously at Princeton's EPPDyL Ref. [10]. In the last year, PT9 was brought to JPL for developmental testing of a new water vapor flow system. However, before testing with water vapor, argon propellant was used with the same operating conditions tested at EPPDyL to verify performance measurements. As shown in Fig. 2, the measured performance is slightly different on individual cases, but within the error bars for both measurements. From this, we can conclude that both facilities provide similar results at similar operating conditions.

## 3.2 PT8 Performance

PT8 was tested with both argon and water vapor propellants in the summer of 1999. Although performance measurements using argon propellant have been presented before [4], results with water vapor have not been presented

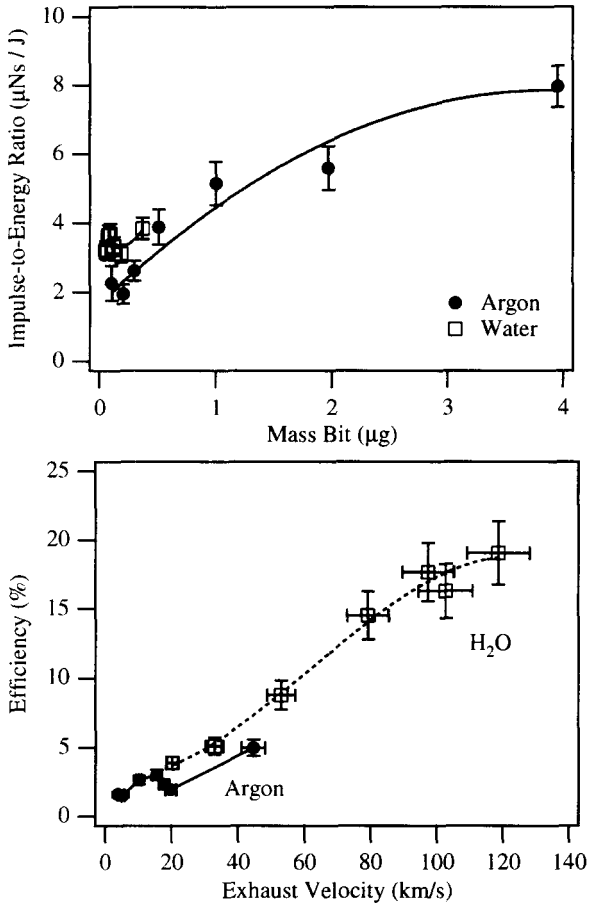


Figure 3: Performance of PT8 using both water vapor and argon for propellants near 2 J/pulse.

until similar trends could be confirmed with a better water vapor flow control system.

As mentioned above, for PT8 the water vapor mass flow rate was held constant using a room temperature water feed system held under low pressure. In those conditions, the upstream pressure is simply the room temperature vapor pressure of water, and the only control of mass bit comes from changing the timing between pulses in a burst. Using this technique, the mass bit was varied between only 0.07-0.3 $\mu$g/pulse. Higher mass bit values could not be reached as longer delays between pulses would permit too much of the propellant to escape beyond the electrode volume. However, argon propellant could be supplied at multiple mass flow rates leading to a wider range of mass bit values, between 0.1-4.0 $\mu$g per pulse.

As shown in Fig. 3, overall performance with water vapor propellant is higher than with argon propellant. However, achievable water mass bit values were much lower than those tested with argon. In erosion rate measurements, we found that approximately 0.1 $\mu$g of electrode was lost per pulse, somewhat greater than the smallest water vapor mass bits. Still, trends show an increasing efficiency with exhaust velocity and a relatively constant impulse-to-energy ratio with water. At higher mass bits, argon propellant performance demonstrates trends previously labeled as "Mode I" behavior in Ref. [6] with an increasing impulse-to-energy ratio and a relatively constant efficiency. This behavior has been noticed before in PT5, a co-axial GFPPT, and PT9 when sidewalls were applied. Although the acceleration process is not as efficient, a higher impulse is produced by confining the propellant within the electrode volume. The ferrite yoke used in PT8 provides nearly a complete sidewall which could explain why the trends found in PT8 at high mass bit match Mode I behavior.

To compare performance of argon and water vapor propellant in the same mode of operation, PT9 provides a better test-bed, as described in the next subsection.

## 3.3 PT9 Performance

The performance of PT9 using argon and water vapor was measured at JPL during the last year. As described at the beginning of this section, the water mass bit can now be varied by a closed-loop temperature control system so the pulse rate (4 kHz) can stay fixed for both propellants.

As shown in Fig. 4, performance using both water vapor and argon propellants exhibit "Mode II" behavior, expected for an electromagnetic acceleration process. In each case, the efficiency increases nearly linearly with exhaust velocity, and the impulse-to-energy ratio is nearly constant over all the mass bit values tested for each propellant. What is also apparent is the increased performance (both efficiency and impulse-to-energy ratio) with the water propellant compared to argon propellant. Although individually each set of argon and water performance points could be argued to be similar within the error bars, there are apparent trends including all the data points together. Based on simple third order polynomial fits of the data, the increase is near 25% for the highest mass bit values (lowest exhaust velocity values) and closer to 15% at the lowest mass bit (highest exhaust velocity). The maximum performance is with water vapor, near 20% efficiency, 70 km/s exhaust velocity, and 6 $\mu Ns/J$.

One point not explicitly brought out in the graphs is the difficultly in initiating the pulse with water vapor propellant. Perhaps because the neutral gas velocity before the pulse is higher with water vapor, less gas may be available near the spark plugs at the breech of the thruster. In any case, there were many more mis-fires with water pro-

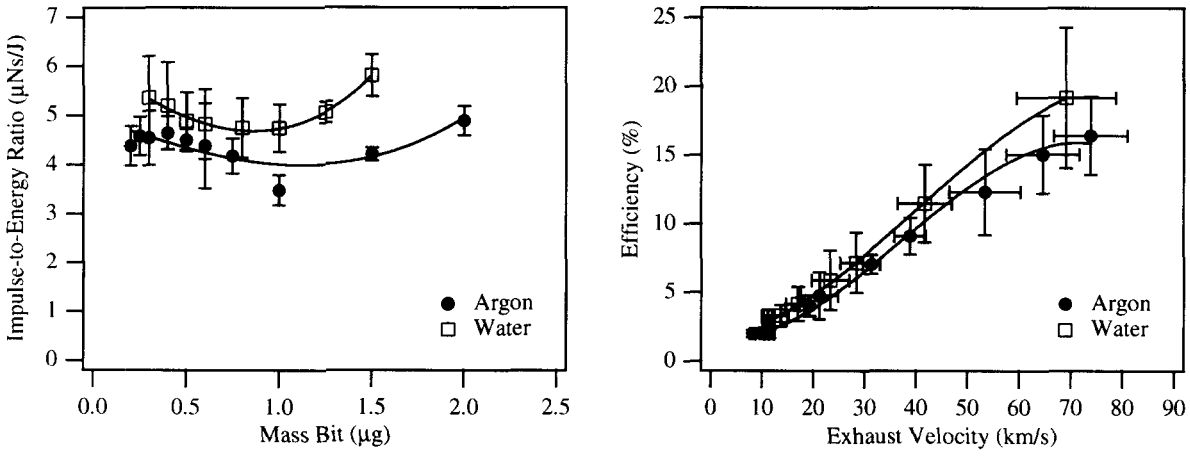


Figure 4: Impulse-to-energy and Efficiency as functions of mass bit and exhaust velocity, respectively, for both argon and water vapor propellants with PT9 near 4 J/pulse. The performance of water vapor is between 15-25% higher than with argon at the same conditions.

pellant creating relatively larger error bars.

# 4 Performance Models

To explain the higher performance found with water vapor propellant, we will now examine two models of electromagnetic acceleration (see Ref. [6]) and current sheet canting (see Ref. [7]). Each model's entire development can be found in the literature, and we will simply use the results here. Following convention, we use the following nomenclature: impulse bit, $I_{bit}$, mass accumulated in the discharge, $m$, current sheet axial velocity, $u$, inductance-per-unit-length, $L^{'}$, total current, $J$, energy stored for each pulse, $E$, capacitance, $C$, initial inductance, $L_0$, and effective plasma resistance, $R$.

## 4.1 Electromagnetic Acceleration

In Ref. [6], a one-dimensional model for the impulse created by the current waveform of a close to critically damped LRC circuit provided the following results,

$$I_{bit} = \int_0^{t_{final}} \left[\frac{d}{dt}(mu)\right] dt, \quad (1)$$

$$= \frac{1}{2}L^{'}\int_0^{t_{final}} J^2 dt, \quad (2)$$

$$= \frac{2}{3}EL^{'}\sqrt{\frac{C}{L_0}}\, f_J(\psi), \quad (3)$$

$$\approx \frac{2E}{U}\, e^{-\sqrt{\psi}}. \quad (4)$$

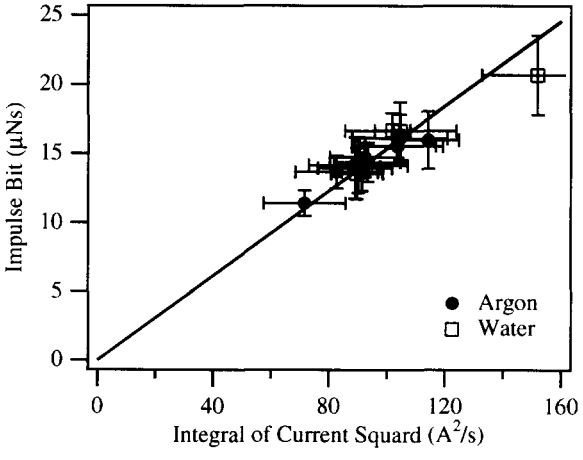


Figure 5: Impulse bit as a function of the integral of the current squared ($\int J^2 dt$). Two lines are shown as the least squares fit to both argon and water vapor propellant data.

where $f_J(\psi)$, the critical resistance ratio, $\psi$, and the GFPPT characteristic velocity, $U$ are defined as,

$$f_J(\psi) \equiv e^{-\left(\frac{\psi}{\sqrt{1-\psi^2}}\sin^{-1}\left(\sqrt{1-\psi^2}\right)\right)} \approx e^{-\sqrt{\psi}}, \quad (5)$$

$$\psi \equiv \frac{R}{2}\sqrt{\frac{C}{L_0}}, \quad (6)$$

$$U \equiv \frac{3}{L^{'}}\sqrt{\frac{L_0}{C}}. \quad (7)$$

Note that the impulse bit is expected to be linearly de-

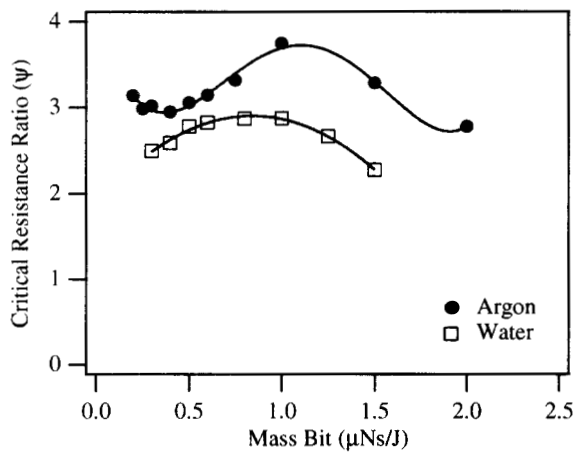


Figure 6: Critical resistance ratio ($\psi$) as a function of mass bit for both argon and water vapor propellants.

pendent on the inductance-per-unit-length and the integral of the total discharge current squared. As shown in Fig. 5, both argon and water vapor propellants exhibit this trait. In fact, using two unique least-squares linear fits to both propellant types yields almost the same slope (both lines are shown on Fig. 5). The slope of the line is nearly $L^{'}/2$, as expected, indicating the thruster is operating in an electromagnetic acceleration mode.

The efficiency provided by this model is linearly proportional to the exhaust velocity,

$$\eta_t \equiv \frac{I_{bit}^2}{2m_{bit}E}, \tag{8}$$

$$= \frac{1}{3}L^{'}\sqrt{\frac{C}{L_0}}\, u_e\, f_J(\psi), \tag{9}$$

$$\approx \frac{u_e}{U}\, e^{-\sqrt{\psi}}.. \tag{10}$$

$$\tag{11}$$

This trend can also be seen in the data (see Fig. 4), yet there is a noticeable difference between the two propellants. According to this model, the difference must be related to the value of the critical resistance ratio, $\psi$, and ultimately the effective plasma resistance. A lower value of $\psi$ or $R$ would lead to higher values of peak current and a larger integral of the current squared. This can already been seen in Fig. 5 where water vapor data has both a higher impulse bit and an integral of the current squared. We will now examine this trend in more detail in the next subsection.

## 4.2 Effective Plasma Resistance

The critical resistance ratio and the effective plasma resistance can be evaluated by using Eq. (3), Eq. (5), and measurements of the impulse-to-energy ratio,

$$f_J(\psi) = \frac{I_{bit}}{E}\frac{U}{2}. \tag{12}$$

This has been done for PT9, and the calculations are shown in Fig. 6. Between the two propellant types, the trends are similar in that $\psi$ increases to a peak value at some mass bit and then decreases again. Also, it is clear that the critical resistance ratio is smaller for water vapor compared to argon, indicating a higher effective plasma resistance for argon. Using measured values of capacitance and initial inductance, the effective plasma resistance is between 40-80 $m\Omega$, which is slightly higher than expected based on pervious GFPPT resistance measurements at higher energy Ref. [7]. Still, using a Spitzer conductivity relation, we could expect that trend since operating at lower energy could result in a lower electron temperature and a higher resistivity. Of course, more measurements of electron temperature, magnetic field strength, etc. need to be made before a quantitative discussion of plasma resistivity can take place.

Another way to investigate the effects of the plasma resistance is to place all dependence on capacitance, initial inductance, and resistance on one side of the relation shown above. We define the "performance factor" $\Gamma$ as,

$$\Gamma = f_J(\psi)\sqrt{\frac{C}{L_0}} = \frac{I_{bit}}{E}\frac{3}{2L^{'}}. \tag{13}$$

Note the higher the performance factor, the higher the impulse-to-energy ratio. Figure 7 shows graphs of performance factor as a function of resistance for various ratios of capacitance-to-inductance. First, it can be seen that lower values of the effective resistance lead to higher values of performance factors. Second, higher values of the capacitance to initial inductance ratio also lead to higher performance factors. At lower values of resistance, the performance is more sensitive to $C/L_0$. At higher values of resistance, the performance does not strongly depend on $C/L_0$, which is important for future GFPPT design considerations. Increasing the capacitance beyond a certain amount with a fixed resistance value will eventually lead to little gain. Therefore increasing capacitance must also be accompanied by somehow reducing the effective plasma resistance in order to keep $\psi$ to reasonable values.

This one-dimensional model obviously has limitations. It does not include effects of current sheet canting or permeability. Although models for current sheet permeability are under development, a model for the canting

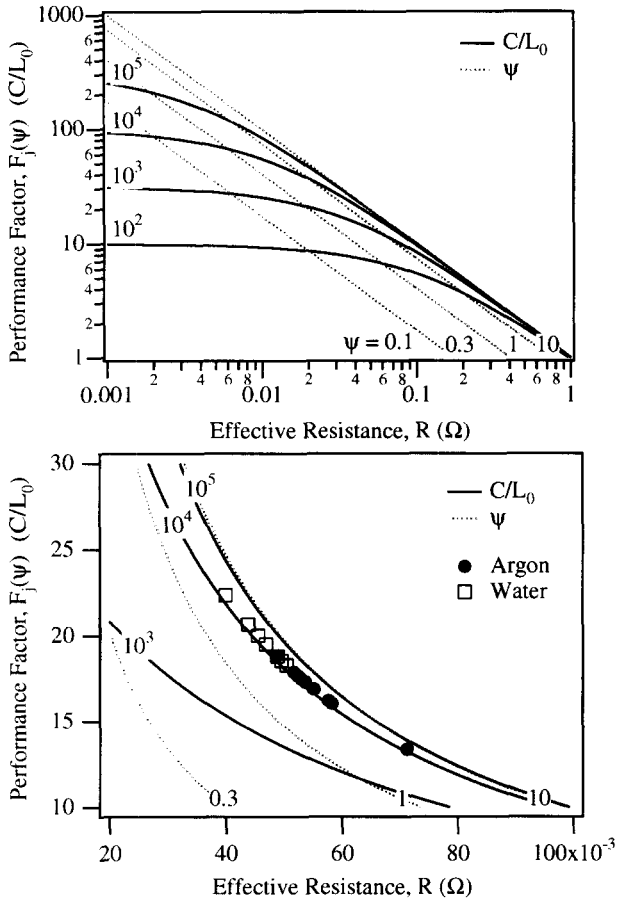


Figure 7: Graphs of performance factor as a function of resistance for various ratios of capacitance-to-inductance. Lines of constant critical resistance ratio ($\psi$) are also shown.

angle in a current sheet has been suggested by Markusic [7]. In the next section we will examine this possibility in more detail.

### 4.3 Current Sheet Canting

Current sheet canting has been observed in many pulsed pulsed plasma devices including the SRL series of GFPPTs [1, 7]. According to a model developed in Ref. [7], canting is initially caused by the expansion of the magnetic field through a propellant starved region near the anode. After a few microseconds, the angle stabilizes due to the competing processes of plasma "pushing" and a Hall effect-induced magnetic field penetration. Measurements of canting angle have been made using a variety of propellants and measurement techniques including magnetic

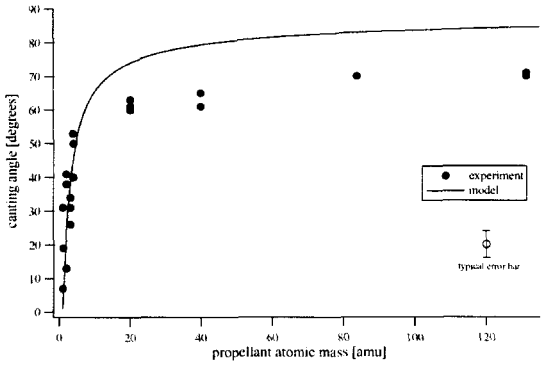


Figure 8: Canting angle as a function of atomic mass. Taken from Markusic Ref. [7] using results from Current Sheet Canting Experiment (CSCX).

field probes, interferometry, and high-speed photography. The results of the measurements along with the model prediction are shown in Fig. 8.

The model developed by Markusic predicts the current sheet canting angle follows this general relation:

$$\theta \propto \tan^{-1}\left(k_1\sqrt{m_w} - k_2\right), \qquad (14)$$

where $k_1$ and $k_2$ are relatively constant with a slight dependence on number density, and $m_w$ is the molecular weight of the propellant. Since the impulse depends on the cosine of the canting angle, small changes in molecular weight can have a significant influence on performance. Using this relation and the data presented in Fig. 8, the impulse should be approximately 20% higher for water propellant compared to argon. In general, this matches the measured performance. Furthermore, Markusic also reports the canting angle decreases for propellants containing hydrogen at higher pressures. For our conditions, the highest pressures exist at the highest mass bit values. Interestingly, the performance improvement using water vapor over argon is highest at the highest mass bit values. Of course, direct measurements of the canting angle in PT9 would be useful for a more quantitative discussion on the effect of canting on performance.

## 5 Conclusions

The performance of a GFPPT using water vapor for propellant has been measured using two different thrusters over a wide range of operational conditions. Measurements taken at Princeton's EPPDyL and the Microthrust Facility at JPL using PT9 showed good agreement for argon propellant at the same operating conditions. In general, the performance using water vapor was found to be

between 15-25% higher compared to using argon. The maximum performance is with water vapor, near 20% efficiency, 70 km/s exhaust velocity, and 6 $\mu Ns/J$. Models of electromagnetic acceleration match well with trends observed in both argon and water vapor data sets. It also appears the effective plasma resistance is higher for argon propellant. A model of current sheet canting also predicts the performance improvement from using a lower molecular weight propellant very near to what was observed. This information should help in designing the next generation GFPPT and improving performance.

## Acknowledgements

The authors would like to acknowledge Tom Markusic and Edgar Choueiri of the Electric Propulsion and Plasma Laboratory at Princeton University for providing data from the CSCX and PT8 performance measurements. The authors also wish to acknowledge Adam Oakes of the Advanced Propulsion Technology Group at JPL for his significant contributions to the experimental setup.

The research described in this paper was carried out at the Jet Propulsion Laboratory, California Institute of Technology, under a contract with the National Aeronautics and Space Administration.

## References

[1] J.K. Ziemer. *Performance Scaling of Gas-Fed Pulsed Plasma Thrusters*. PhD thesis, Princeton University, 2001.

[2] J.K. Ziemer, E.Y. Choueiri, and D. Birx. Is the Gas-Fed PPT an Electromagnetic Accelerator? An Investigation Using Measured Performance. In $35^{th}$ *Joint Propulsion Conference*, Los Angeles, California, June 20-24 1999. AIAA 99-2289.

[3] J. Blandino, D. Birx, J.K. Ziemer, and E.Y. Choueiri. Performance and Erosion Measurements of the PT8 Gas-Fed Pulsed Plasma Thruster. Technical Report EPPDyL-JPL99b, NASA Jet Propulsion Laboratory, August 1999.

[4] J.K. Ziemer, E.Y. Choueiri, and D. Birx. Comparing the Performance of Co-Axial and Parallel-Plate Gas-Fed PPTs. In $26^{th}$ *International Electric Propulsion Conference*, Kitakyushu, JAPAN, October 17-21 1999. IEPC 99-209.

[5] J.K. Ziemer and R.A. Petr. Impact of Performance Scaling on Mission Analysis for Gas-Fed Pulsed Plasma Thrusters. In $27^{th}$ *International Electric Propulsion Conference*, Pasadena, California, October 15-19 2001. IEPC 01-148.

[6] J.K. Ziemer and E.Y. Choueiri. Scaling Laws for Electromagnetic, Pulsed Plasma Thrusters. *PLASMA SOURCES SCIENCE & TECHNOLOGY*, 10(3):395–405, 2001.

[7] T.E. Markusic. *Current Sheet Canting in Pulsed Electromagnetic Accelerators*. PhD thesis, Princeton University, 2002.

[8] J.K. Ziemer. Performance Measurements Using a Sub-Micronewton Resolution Thrust Stand. In $27^{th}$ *International Electric Propulsion Conference*, Pasadena, California, October 15-19 2001. IEPC 01-238.

[9] J.K. Ziemer and E.Y. Choueiri. Performance and Erosion Measurements of Gas-Fed Pulsed Plasma Thrusters at NASA Jet Propulsion Laboratory. Technical Report EPPDyL-JPL99a, Princeton University, March 1999.

[10] J.K. Ziemer and E.Y. Choueiri. A Characteristic Velocity for Gas-Fed PPT Performance Scaling. In $36^{th}$ *Joint Propulsion Conference*, Huntsville, Alabama, July 16-19 2000. AIAA 2000-3432.